# Switching Hydrogen Bonding to π−Stacking: The Thiophenol Dimer and Trimer

Rizalina Tama Saragi,[†] Marcos Juanes,[†] Cristóbal Pérez,[‡] Pablo Pinacho,[‡]
Denis S. Tikhonov,[‡] Walther Caminati,[§] Melanie Schnell,[‡] Alberto Lesarri[†]*

[†]Departamento de Química Física y Química Inorgánica, Facultad de Ciencias - I.U. CINQUIMA, Universidad de Valladolid, Paseo de Belén, 7, E-47011 Valladolid (Spain)

[‡]Deutsches Elektronen-Synchrotron DESY, Notkestraße 85, D-22607 Hamburg (Germany) and Institut für Physikalische Chemie, Christian-Albrechts-Universität zu Kiel, Max-Eyth-Str. 1, D-24118 Kiel (Germany)

[§]Dipartimento di Chimica Giacomo Ciamician, Via Selmi, 2, I-40126 Bologna (Italy)

ABSTRACT: We used jet-cooled broadband rotational spectroscopy to explore the balance between π-stacking and hydrogen bonding interactions in the self-aggregation of thiophenol. Two different isomers were detected for the thiophenol dimer, revealing dispersion-controlled π-stacked structures anchored by a long S-H⋯S sulfur hydrogen bond. The weak intermolecular forces allow for noticeable internal dynamics in the dimers, as tunneling splittings are observed for the global minimum. The large-amplitude motion is ascribed to a concerted inversion motion between the two rings, exchanging the roles of the proton donor and acceptor in the thiol groups. The determined torsional barrier of $B_2$= 250.3 cm$^{-1}$ is consistent with theoretical predictions (290-502 cm$^{-1}$) and the monomer barrier of 277.1(3) cm$^{-1}$. For the thiophenol trimer, a symmetric top structure was assigned in the spectrum. The results highlight the relevance of substituents effects to modulate π-stacking geometries and the role of the sulfur-centered hydrogen bonds.

**TOC GRAPHICS**
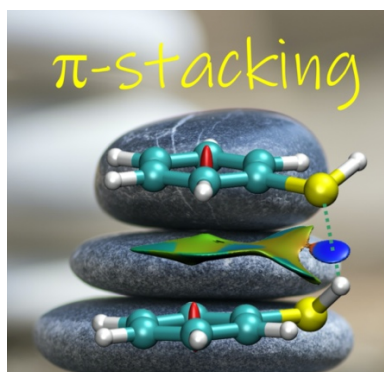


**KEYWORDS**: π-Stacking, Molecular recognition, Intermolecular interactions, Sulfur Hydrogen bonding, Rotational spectroscopy, Jet spectroscopy, Thiophenol.

$\pi$–Stacking forces are fascinating interactions with a misguiding name, leading some authors to dismiss this term.[1,2] Non-covalent interactions between neutral closed-shell unsaturated organic groups are decisive contributors to biochemical structures, as in DNA/RNA nucleobase stacking or protein folding.[3–5] In addition, the influence of stacking forces extends to organic and organometallic synthesis,[6] protein and crystal design,[7] host-guest compounds,[8] catalysis,[9] materials,[10] and supramolecular Chemistry,[6] calling for a description at molecular level.

The polar electrostatic or Hunter-Sanders[11] model initially ascribed $\pi$-stacking to quadrupole-quadrupole interactions ($1/r^7$ distance dependence). However, more recent computational analyses[1,2] using energy decomposition attribute the physical origin of $\pi$–$\pi$ stacking stabilization to dispersion forces ($1/r^6$ dependence), promoted by the close near-parallel biplanar arrangement. The quadrupolar electrostatic potential actually favors stacking of saturated rings, but this factor is counterbalanced by a reduced Pauli exchange repulsion for arene-arene stacking. Other calculations have explored the balance between dispersion and electrostatic effects[12–14] or revealed the connection of dispersion and DNA helicity.[15] However, since arene stacking stabilization is not based upon direct $\pi$-cloud attraction the concept of "$\pi$-stacking" should only be used as positional descriptor.

Experiments on stacking are crucial to validate the increasingly complex theoretical models. In particular, gas-phase experiments are unbiased by perturbing matrix effects and directly comparable to the computational predictions. As an illustrative example, the rotational spectrum of the benzene dimer contributed to the theoretical dispute between the observed T-shape[16–18] and the alternative parallel geometry.[19] Most of gas-phase stacking experiments have used double-resonance IR-UV spectroscopy,[20–24] but their vibrational signatures are usually of low resolution. Microwave spectroscopy provides accurate structural descriptions through the moments of inertia.[25,26] However,

there are just a few rotational investigations of π-stacking clusters. For a single benzene ring, the serendipitous observation of the 1,2-difluorobenzene dimer[27] benefited from the changes in the molecular electrostatic potential due to strongly electronegative substituents, but it took years to realize the correct geometry. For two fused rings, dibenzofuran[28] and 1-napthol[29] exhibit stacking, consistent with the increased stability of larger arene dimers.[1]

Apart from fluorination, other weaker substituent effects,[12,13] like fine-tuning of hydrogen bonding, can be explored to switch single-ring dimers from non-stacking into stacking. In the case of phenol, the dimer[30,31] is controlled by a moderately strong O-H···O hydrogen bond that results in a "hinged" structure intermediate between T or stacked geometries, very sensitive to dispersion contributions.[32] The dimer of aniline shows the opposite effect, with a (head-to-tail) apolar antiparallel stacking and no N-H···N hydrogen bond between the amino groups (Figure 1).[33] Here, we explore the replacement of oxygen in phenol by a heavier less-electronegative chalcogen atom like sulfur, proving that it maintains S-H···S hydrogen bonding while simultaneously resulting in a π-stacking homodimer. The work is extended also to the thiophenol trimer, complementing our view on sulfur hydrogen bonding[34–37] and allowing comparisons with the phenol[31] and aniline[38] trimers.

The experiment was assisted by several computational models described in Supporting information (SI). We present results based on four DFT methods, including hybrid (B3LYP, ωB97XD, PBEh-3c) and double-hybrid (B2PLYP) functionals with empirical dispersion corrections.[39] The B3LYP-D3(BJ) dimer calculations of Table S1 (SI) converged to eight structures, with four isomers at electronic energies below 1.4 kJ mol$^{-1}$ and four additional species in the 2-5 kJ mol$^{-1}$ range. The four most stable structures were reoptimized with B2PLYP-D3(BJ) (Table 1) and ωB97XD (Table S2, SI) to check

the computational consistency. For the trimer, B3LYP-D3(BJ) predicted two practically isoenergetic isomers (Table S3, SI), while six other structures were found at electronic energies below 5 kJ mol$^{-1}$. The two most stable trimer isomers were similarly reoptimized with B2PLYP-D3(BJ) and ωB97XD in Tables 2 and S4 (SI). All reported species are local minima at their calculation level.

The experimental investigation used supersonic-jet chirped-pulsed Fourier-transform microwave[40] (CP-FTMW) spectrometers in Valladolid and Hamburg, operating in the region 2-8 GHz (see SI). CP-FTMW spectroscopy is a rotational coherence technique using MW linear fast-passage excitation to activate molecular rotational resonances, later recording the time-domain free-induction decay caused by rotational dephasing. The experiment requires fast electronics to tackle the stringently short (μs) excitation times, but the resulting spectra provide full-bandwidth and high dynamical range capabilities which turn out essential for the analysis of complicated congested spectra.

The observed rotational spectrum in Figures 2 and S1 (SI) is dominated by intense monomer transitions, previously reported.[41] Similarly to phenol, thiophenol tunnels between two equivalent planar structures connected by the internal rotation of the thiol group, splitting the ground vibrational state into two torsional-rotation sublevels (Table S5, SI). However, the internal rotation barrier is much smaller than in phenol, i.e. 277.1(3) cm$^{-1}$ vs. 1213 cm$^{-1}$.[42] For the thiophenol dimer, two different asymmetric rotors were assigned in the spectrum. Isomer I exhibited only $\mu_b$ transitions and behaved like a semi-rigid rotor, so it could be fitted using a Watson's semi-rigid rotor Hamiltonian.[43] Isomer II presented $\mu_b$ transitions with small (<0.5 MHz) tunneling doublings, indicative of an internal large-amplitude motion (LAM) connecting two symmetry-equivalent structures. A second set of $\mu_c$ transitions showed larger tunnelling splittings (ca. 17 MHz), near

independent of the angular momentum quantum number. This fact suggested a $\mu_c$-inverting motion, so the experimental transitions were fitted to a two-state rovibrational Hamiltonian without Coriolis coupling terms. For the trimer, we found a set of transitions corresponding to the pattern of a symmetric rotor, but we could not resolve the $K$ quantum number fine structure. The experimental frequencies of the rotational transitions are collected in Tables S6-S8 (SI).

The comparison between experiment and theory in Tables 1-2 and S1-S4 (SI) allowed the identification of the spectral carriers. The predictions suggest parallel displaced (PD) dimer geometries, all sustained by an intermolecular hydrogen bond S-H$\cdots$S. Two alternative slipped structures are predicted depending on the relative orientation of the phenyl ring with respect to the linking thiol groups, denoted PD1 and PD2 in Figure 1 and 3D Figures S2-S3 (SI). Moreover, for each ring geometry, two isomers arise differing on the parallel (*cis*) or antiparallel (*trans*) orientation of the terminal thiol groups, so four isomers are finally predicted for the dimer. Isomer I was identified as PD1-*trans* based on the rotational constants and dominance of the $\mu_b$-dipole moment component. Similarly, the $\mu_c$ spectrum led to the assignment of isomer II as PD2-*cis*. The internal dynamics of PD2-*cis* was attributed to a concerted motion of thiol inversion, which exchanges the proton donor and acceptor moieties (Figure S4 and multimedia, SI). The inversion barrier was determined from the experimental tunnelling splitting $\Delta E_{01}$=8.8698(51) MHz using Meyer's flexible model.[44] Following consideration of the main structural relaxations associated to the C-S bond (see SI) the experiment was reproduced for a potential barrier of $B_2$= 250.3 cm$^{-1}$. We compared this barrier with a computational prediction of the torsional potential using DFT and the nudged elastic band algorithm[45] (SI). The results for three DFT functionals in Table S9 and Figures S5-S6 (SI) range from 290 ($\omega$B97X-D3) to 502 cm$^{-1}$ (B3LYP-D3), giving rise to estimated

tunnelling splittings of 13, 4 and 525 MHz (PBEh-3c, B3LYP-D3 and ωB97X-D3, respectively). These calculations confirm a torsional barrier similar to the monomer. A lack of double-minimum symmetry prevents tunneling effects for isomer PD1.

The dimer global minimum was identified with a second experiment using argon as carrier gas, checking the possibility of conformational relaxation with more energetic intermolecular jet collisions. The weaker argon spectrum, illustrated in Figures 3 and S7 (SI), revealed no signals from PD1 and established PD2 as the global minimum. For the thiophenol trimer, the symmetric rotor (UUU in Tables 2, S3 and Figure S8, SI), characterized by three consecutive S-H$\cdots$S hydrogen bonds, can be associated to the observed transitions. No other species could be identified positively, but we do not exclude the presence of other species because of additional unidentified lines.

A coherent picture emerges from the present experiment concerning the correlation between thiophenol aggregation and non-covalent interactions. For the thiophenol dimer, the calculations suggest two alternative clustering mechanisms, based either on S-H$\cdots$S or S-H$\cdots\pi$ hydrogen bonds. While the relative energies for the first eight isomers are quite close, the preference for a combination of S-H$\cdots$S hydrogen bond and $\pi$-stacking is notorious, offering insight into their structural, energetic and physical properties. The parallel-displaced global minimum PD2-*cis* exhibits a long hydrogen bond (B2PLYP: $r$(S-H$\cdots$S)=2.84 Å) with considerable non-linearity ($\angle$(S-H$\cdots$S)=134.5°). Similar values are presented for PD1 in Figure 1 (molecular structures in Tables S10-S13, and 3D Figures S2-S3, SI). This bonding distance is slightly larger than the hydrogen sulfide dimer[46] prototype ($r$(S-H$\cdots$S)=2.778(9) Å) and qualitatively reflects the gradation of hydrogen bond strength observed in the dimers of $H_2S$-$H_2O$[47] ($r$(O-H$\cdots$S)=2.597(4) Å), $H_2O$-$H_2S$[47] ($r$(S-H$\cdots$O)=2.195 Å) and $(H_2O)_2$[48] ($r$(O-H$\cdots$O)=1.951 Å) in Table S14 (SI). Thiol-alcohol gas-phase hydrogen bonds were also

reported for the monohydrates of furfuryl[36] and thenyl[37] mercaptan ($r$(S-H···O)=2.22-2.44 Å; $r$(O-H···S)=2.43-2.58 Å), but the experimental investigations of gas-phase hydrogen bonds between thiols are still scarce.[34,35] Protein crystal contacts between the cysteine thiol and the sulfur atom in methionine or cysteine have shorter average values of $r$(S-H···S)=2.55(47) Å.[49]

The π-stacking geometry of the thiophenol dimers is characterized by the distance between centroids ($d$) and angle between aromatic planes ($\phi$). The interplanar distances, shorter for PD2 (B2PLYP: $d$(PD2)=3.41-3.42 Å < $d$(PD1)=3.76-3.77 Å), and the ring orientations (B2PLYP: $\phi$(PD2)=2.9°-4.4° < $\phi$(PD1)=9.2°-10.2°) nicely match previous structural surveys of protein-ligand interactions between aromatic groups, confirming a common binding pattern.[50] For the trimer, the final geometry in Figure S8 and Table S15 (SI) balances both S-H···S and C-H···π interactions, as in phenol and aniline, with an hydrogen bond distance of $r$(S-H···S)=2.75 Å (B2PLYP).

The physical origin of the non-covalent interactions was modelled by a topological analysis of the reduced electronic density gradient $s$ $\left(= \frac{1}{2(3\pi^2)^{1/3}} \frac{|\nabla\rho|}{\rho^{4/3}}\right)$ and energy decomposition. NCI plots in Figures 4, 5, and S9 (SI) indicate a confluence of the S-H···S hydrogen bond and delocalized interaction regions in between the aromatic rings, consistent with the observed geometries. A binding energy decomposition using Symmetry-Adapted Perturbation Theory SAPT 2+(3) in Figure 6 and Table S16 (SI) offers comparison with phenol and aniline. The SAPT 2+(3) binding energy of the thiophenol dimer (PD1: -25.9 kJ mol$^{-1}$; PD2: -26.9 kJ mol$^{-1}$) is only 1-2 kJ mol$^{-1}$ smaller than in the phenol dimer (-27.6 kJ mol$^{-1}$). However, it shows a much larger dispersion component than in phenol, accounting for 185.2% (PD1) or 198.5% (PD2) of the total binding energy, close to the contribution in the van der Waals dimer of pyridine-methane (208.1%). In parallel, the electrostatic contribution in thiophenol is reduced to 96.4%

(PD1) and 97.4% (PD2) of the binding energy, compared to 151.3% in the phenol dimer or 57.5% in pyridine-methane.

In conclusion, chirped-pulse rotational spectroscopy opens new avenues for the investigation of increasingly larger adducts, simultaneously offering striking comparison with low-resolution IR studies.[51] We observed two isomers of the thiophenol dimer, confirming two different π-stacking structures assisted by a long S-H···S hydrogen bond. The dimer geometries reveal flexible internal dynamics, as two different geometries are simultaneously detected, and one of the isomers exhibits an internal large-amplitude motion causing spectral doublings. The experiment also provided empirical evidence to contrast the computational models. The three DFT model predictions were comparable in structural terms, with relative deviations from the experimental rotational constants of 0.2-3.5% (ωB97XD), 0.2-4.0% (B3LYP-D3) and 0.3-4.4% (B2PLYP-D3). The ωB97XD/cc-PVTZ binding energies, previously claimed similar to CCSD(T) for aromatic homodimers,[50] differ less than 1 kJ mol$^{-1}$ from B2PLYP-D3, with B3LYP-D3 giving larger values by 3-4 kJ mol$^{-1}$. The moderate interaction energies and the energy decomposition balance evidence that the thiophenol dimer represents an interesting case of coexistence of electrostatic and dispersion interactions, with the primary S-H···S hydrogen bond acting as molecular anchor for positioning of the phenyl rings. The geometry of the trimer maintains the preference for a cooperative hydrogen bond network as observed in phenol and aniline, but the $C_3$ symmetry reflects a delicate balance between the hydrogen bond and C-H···π interactions and may not be present in other trimers. The results emphasize the role of substituents effects to modulate π-stacking geometries and the importance of sulfur-centered hydrogen bonds. The connection between gas-phase aggregation processes and the design of supramolecular architectures remains a challenge for future studies.

## ASSOCIATED CONTENT

### Supporting Information

The Supporting Information is available free of charge on the ACS Publications website at DOI: 10.1021…

Experimental and theoretical methods; Figures S1-S9; Tables S1-S16.

## AUTHOR INFORMATION

### Corresponding author

*E-mail: alberto.lesarri@uva.es

### Notes

The authors declare no competing financial interest.

## REFERENCES

(1)     Grimme, S. Do Special Noncovalent π-π Stacking Interactions Really Exist? *Angew. Chemie - Int. Ed.* **2008**, *47* (18), 3430–3434. https://doi.org/10.1002/anie.200705157.

(2)     Martinez, C. R.; Iverson, B. L. Rethinking the Term "π-Stacking." *Chem. Sci.* **2012**, *3* (7), 2191–2201. https://doi.org/10.1039/c2sc20045g.

(3)     Burley, S.; Petsko, G. Aromatic-Aromatic Interaction: A Mechanism of Protein Structure Stabilization. *Science (80-. ).* **1985**, *229* (4708), 23–28. https://doi.org/10.1126/science.3892686.

(4)     McGaughey, G. B.; Gagné, M.; Rappé, A. K. π-Stacking Interactions, Alive and Well in Proteins. *J. Biol. Chem.* **1998**, *273* (25), 15458–15463. https://doi.org/10.1074/jbc.273.25.15458.

(5)     Kool, E. T. Hydrogen Bonding, Base Stacking, and Steric Effects in DNA Replication. *Annu. Rev. Biophys. Biomol. Struct.* **2001**, *30* (1), 1–22. https://doi.org/10.1146/annurev.biophys.30.1.1.

(6)     *Non-Covalent Interactions in the Synthesis and Design of New Compounds*; Maharramov, A. M., Mahmudov, K. T., Kopylovich, M. N., Pombeiro, A. J. L., Eds.; John Wiley & Sons, Inc: Hoboken, NJ, 2016. https://doi.org/10.1002/9781119113874.

(7)     Stornaiuolo, M.; De Kloe, G. E.; Rucktooa, P.; Fish, A.; Van Elk, R.; Edink, E. S.; Bertrand, D.; Smit, A. B.; De Esch, I. J. P.; Sixma, T. K. Assembly of a π-π Stack of Ligands in the Binding Site of an Acetylcholine-Binding Protein. *Nat. Commun.* **2013**, *4* (May). https://doi.org/10.1038/ncomms2900.

(8)     Salonen, L. M.; Ellermann, M.; Diederich, F. Aromatic Rings in Chemical and Biological Recognition: Energetics and Structures. *Angew. Chemie - Int. Ed.* **2011**, *50* (21), 4808–4842. https://doi.org/10.1002/anie.201007560.

(9)     Neel, A. J.; Hilton, M. J.; Sigman, M. S.; Toste, F. D. Exploiting Non-Covalent π Interactions for Catalyst Design. *Nature* **2017**, *543* (7647), 637–646. https://doi.org/10.1038/nature21701.

(10)    Schlosser, F.; Moos, M.; Lambert, C.; Würthner, F. Redox-Switchable Intramolecular π-π-Stacking of Perylene Bisimide Dyes in a Cyclophane. *Adv. Mater.* **2013**, *25* (3), 410–414. https://doi.org/10.1002/adma.201201266.

(11)    Hunter, C. A.; Sanders, J. K. M. The Nature of π-π Interactions. *J. Am. Chem. Soc.* **1990**, *112* (14), 5525–5534. https://doi.org/10.1021/ja00170a016.

(12)    Wheeler, S. E.; Houk, K. N. Substituent Effects in the Benzene Dimer Are Due to Direct Interactions of the Substituents with the Unsubstituted Benzene. *J. Am. Chem. Soc.* **2008**, *130* (33), 10854–10855. https://doi.org/10.1021/ja802849j.

(13)    Riwar, L. J.; Trapp, N.; Kuhn, B.; Diederich, F. Substituent Effects in Parallel-Displaced π–π Stacking Interactions: Distance Matters. *Angew. Chemie - Int. Ed.* **2017**, *56* (37), 11252–11257. https://doi.org/10.1002/anie.201703744.

(14)    Watt, M.; Hardebeck, L. K. E.; Kirkpatrick, C. C.; Lewis, M. Face-to-Face Arene-Arene Binding Energies: Dominated by Dispersion but Predicted by Electrostatic and Dispersion/Polarizability Substituent Constants. *J. Am. Chem. Soc.* **2011**, *133* (11), 3854–3862. https://doi.org/10.1021/ja105975a.

(15)    Černý, J.; Kabeláč, M.; Hobza, P. Double-Helical → Ladder Structural Transition in the B-DNA Is Induced by a Loss of Dispersion Energy. *J. Am. Chem. Soc.* **2008**, *130* (47), 16055–16059. https://doi.org/10.1021/ja805428q.

(16)    Arunan, E.; Gutowsky, H. S. The Rotational Spectrum, Structure and Dynamics of a Benzene Dimer. *J. Chem. Phys.* **1993**, *98* (5), 4294–4296.

https://doi.org/10.1063/1.465035.

(17) Schnell, M.; Erlekam, U.; Bunker, P. R.; Vonhelden, G.; Grabow, J.-U.; Meijer, G.; Vanderavoird, A. Structure of the Benzene Dimer - Governed by Dynamics. *Angew. Chemie - Int. Ed.* **2013**, *52* (19), 5180–5183. https://doi.org/10.1002/anie.201300653.

(18) Schnell, M.; Erlekam, U.; Bunker, P. R.; Von Helden, G.; Grabow, J.-U.; Meijer, G.; Van Der Avoird, A. Unraveling the Internal Dynamics of the Benzene Dimer: A Combined Theoretical and Microwave Spectroscopy Study. *Phys. Chem. Chem. Phys.* **2013**, *15* (25), 10207–10223. https://doi.org/10.1039/c3cp51181b.

(19) Sinnokrot, M. O.; Sherrill, C. D. Highly Accurate Coupled Cluster Potential Energy Curves for the Benzene Dimer: Sandwich, T-Shaped, and Parallel-Displaced Configurations. *J. Phys. Chem. A* **2004**, *108* (46), 10200–10207. https://doi.org/10.1021/jp0469517.

(20) Busker, M.; Svartsov, Y. N.; Häber, T.; Kleinermanns, K. IR-UV Double Resonance Spectra of Pyrazine Dimers: Competition between CH ⋯ π, π ⋯ π and CH ⋯ N Interactions. *Chem. Phys. Lett.* **2009**, *467* (4–6), 255–259. https://doi.org/10.1016/j.cplett.2008.10.091.

(21) Pietraperzia, G.; Pasquini, M.; Schiccheri, N.; Piani, G.; Becucci, M.; Castellucci, E.; Biczysko, M.; Bloino, J.; Barone, V. The Gas Phase Anisole Dimer: A Combined High-Resolution Spectroscopy and Computational Study of a Stacked Molecular System. *J. Phys. Chem. A* **2009**, *113* (52), 14343–14351. https://doi.org/10.1021/jp903236z.

(22) Maity, S.; Patwari, G. N.; Sedlak, R.; Hobza, P. A π-Stacked Phenylacetylene Dimer. *Phys. Chem. Chem. Phys.* **2011**, *13* (37), 16706–16712. https://doi.org/10.1039/c1cp20677j.

(23) Kundu, A.; Sen, S.; Patwari, G. N. The Propargylbenzene Dimer: C-H⋯π Assisted π-π Stacking. *Phys. Chem. Chem. Phys.* **2015**, *17* (14), 9090–9097. https://doi.org/10.1039/c5cp00162e.

(24) Mondal, S. I.; Sen, S.; Hazra, A.; Patwari, G. N. π-Stacked Dimers of Fluorophenylacetylenes: Role of Dipole Moment. *J. Phys. Chem. A* **2017**, *121* (18), 3383–3391. https://doi.org/10.1021/acs.jpca.7b00209.

(25) Caminati, W.; Grabow, J.-U. Advancements in Microwave Spectroscopy. In *Frontiers and Advances in Molecular Spectroscopy*; Laane, J., Ed.; Elsevier Inc., 2018; pp 569–598. https://doi.org/10.1016/B978-0-12-811220-5.00018-6.

(26) Juanes, M.; Saragi, R. T.; Caminati, W.; Lesarri, A. The Hydrogen Bond and Beyond: Perspectives for Rotational Investigations of Non-Covalent Interactions. *Chem. - A Eur. J.* **2019**, *25* (49), 11402–11411. https://doi.org/10.1002/chem.201901113.

(27) Goly, T.; Spoerel, U.; Stahl, W. The Microwave Spectrum of the 1,2-Difluorobenzene Dimer. *Chem. Phys.* **2002**, *283* (1–2), 289–296. https://doi.org/10.1016/S0301-0104(02)00500-1.

(28) Fatima, M.; Steber, A. L.; Poblotzki, A.; Pérez, C.; Zinn, S.; Schnell, M. Rotational Signatures of Dispersive Stacking in the Formation of Aromatic Dimers. *Angew. Chemie - Int. Ed.* **2019**, *58* (10), 3108–3113. https://doi.org/10.1002/anie.201812556.

(29) Seifert, N. A.; Hazrah, A. S.; Jäger, W. The 1-Naphthol Dimer and Its Surprising Preference for π-π Stacking over Hydrogen Bonding. *J. Phys. Chem. Lett.* **2019**, *10* (11), 2836–2841. https://doi.org/10.1021/acs.jpclett.9b00646.

(30) Schmitt, M.; Böhm, M.; Ratzer, C.; Krügler, D.; Kleinermanns, K.; Kalkman, I.; Berden, G.; Meerts, W. L. Determining the Intermolecular Structure in the S0

and S1 States of the Phenol Dimer by Rotationally Resolved Electronic Spectroscopy. *ChemPhysChem* **2006**, *7* (6), 1241–1249. https://doi.org/10.1002/cphc.200500670.

(31) Seifert, N. A.; Steber, A. L.; Neill, J. L.; Pérez, C.; Zaleski, D. P.; Pate, B. H.; Lesarri, A. The Interplay of Hydrogen Bonding and Dispersion in Phenol Dimer and Trimer: Structures from Broadband Rotational Spectroscopy. *Phys. Chem. Chem. Phys.* **2013**, *15* (27), 11468–11477. https://doi.org/10.1039/c3cp51725j.

(32) Hobza, P.; Muller-Dethlefs, K. *Non-Covalent Interactions*; Hobza, P., Muller-Dethlefs, K., Eds.; Theoretical and Computational Chemistry Series; Royal Society of Chemistry: Cambridge, 2009. https://doi.org/10.1039/9781847559906.

(33) Sugawara, K. I.; Miyawaki, J.; Nakanaga, T.; Takeo, H.; Lembach, G.; Djafari, S.; Barth, H. D.; Brutschy, B. Infrared Depletion Spectroscopy of the Aniline Dimer. *J. Phys. Chem.* **1996**, *100* (43), 17145–17147. https://doi.org/10.1021/jp961901q.

(34) Biswal, H. S.; Bhattacharyya, S.; Bhattacherjee, A.; Wategaonkar, S. Nature and Strength of Sulfur-Centred Hydrogen Bonds: Laser Spectroscopic Investigations in the Gas Phase and Quantum-Chemical Calculations. *Int. Rev. Phys. Chem.* **2015**, *34* (1), 99–160. https://doi.org/10.1080/0144235X.2015.1022946.

(35) Juanes, M.; Saragi, R. T.; Jin, Y.; Zingsheim, O.; Schlemmer, S.; Lesarri, A. Rotational Spectrum and Intramolecular Hydrogen Bonding in 1,2-Butanedithiol. *J. Mol. Struct.* **2020**, *1211*, 128080. https://doi.org/10.1016/j.molstruc.2020.128080.

(36) Juanes, M.; Lesarri, A.; Pinacho, R.; Charro, E.; Rubio, J. E.; Enríquez, L.; Jaraíz, M. Sulfur Hydrogen Bonding in Isolated Monohydrates: Furfuryl Mercaptan versus Furfuryl Alcohol. *Chem. - A Eur. J.* **2018**, *24* (25), 6564–6571. https://doi.org/10.1002/chem.201705727.

(37) Juanes, M.; Saragi, R. T.; Pinacho, R.; Rubio, J. E.; Lesarri, A. Sulfur Hydrogen Bonding and Internal Dynamics in the Monohydrates of Thenyl Mercaptan and Thenyl Alcohol. *Phys. Chem. Chem. Phys.* **2020**, *22* (22), 12412–12421. https://doi.org/10.1039/D0CP01706J.

(38) Pérez, C.; León, I.; Lesarri, A.; Pate, B. H.; Martínez, R.; Millán, J.; Fernández, J. A. Isomerism of the Aniline Trimer. *Angew. Chemie - Int. Ed.* **2018**, *57* (46), 15112–15116. https://doi.org/10.1002/anie.201808602.

(39) Grimme, S.; Ehrlich, S.; Goerigk, L. Effect of the Damping Function in Dispersion Corrected Density Functional Theory. *J. Comput. Chem.* **2011**, *32* (7), 1456–1465. https://doi.org/10.1002/jcc.21759.

(40) Shipman, S. T.; Pate, B. H. New Techniques in Microwave Spectroscopy. In *Handbook of High-resolution Spectroscopy*; Merkt, F., Quack, M., Eds.; Major Reference Works; John Wiley & Sons, Ltd: New York, 2011; pp 801–828. https://doi.org/10.1002/9780470749593.hrs036.

(41) Larsen, N. W.; Schulz, L. Internal Rotation and Structure of Thiophenol and 4-Fluorothiophenol Studied by Microwave Spectroscopy and Quantum Chemistry. *J. Mol. Struct.* **2009**, *920* (1–3), 30–39. https://doi.org/10.1016/j.molstruc.2008.10.015.

(42) Larsen, N. W.; Nicolaisen, F. M. Far-Infrared Gas Spectra of Phenol, 4-Fluorophenol, Thiophenol and Some Deuterated Species: Barrier to Internal Rotation. *J. Mol. Struct.* **1974**, *22* (1), 29–43. https://doi.org/10.1016/0022-2860(74)80065-7.

(43) Watson, J. K. G. Aspects of Quartic and Sextic Centrifugal Effects on Rotational Energy Levels. In *Vibrational Spectra and Structure, vol. 6*; Durig, J. R., Ed.;

Elsevier B.V.: Amsterdam, 1977; pp 1–89.

(44)   Meyer, R. Flexible Models for Intramolecular Motion, a Versatile Treatment and Its Application to Glyoxal. *J. Mol. Spectrosc.* **1979**, *76* (1–3), 266–300. https://doi.org/10.1016/0022-2852(79)90230-3.

(45)   Mills, G.; Jónsson, H.; Schenter, G. K. Reversible Work Transition State Theory: Application to Dissociative Adsorption of Hydrogen. *Surf. Sci.* **1995**, *324* (2–3), 305–337. https://doi.org/10.1016/0039-6028(94)00731-4.

(46)   Das, A.; Mandal, P. K.; Lovas, F. J.; Medcraft, C.; Walker, N. R.; Arunan, E. The H2S Dimer Is Hydrogen-Bonded: Direct Confirmation from Microwave Spectroscopy. *Angew. Chemie Int. Ed.* **2018**, *57* (46), 15199–15203. https://doi.org/10.1002/anie.201808162.

(47)   Lovas, F. J. *Private Communication*; 2020.

(48)   Mukhopadhyay, A.; Cole, W. T. S.; Saykally, R. J. The Water Dimer I: Experimental Characterization. *Chem. Phys. Lett.* **2015**, *633*, 13–26. https://doi.org/10.1016/j.cplett.2015.04.016.

(49)   Zhou, P.; Tian, F.; Lv, F.; Shang, Z. Geometric Characteristics of Hydrogen Bonds Involving Sulfur Atoms in Proteins. *Proteins Struct. Funct. Bioinforma.* **2009**, *76* (1), 151–163. https://doi.org/10.1002/prot.22327.

(50)   Huber, R. G.; Margreiter, M. A.; Fuchs, J. E.; Von Grafenstein, S.; Tautermann, C. S.; Liedl, K. R.; Fox, T. Heteroaromatic π-Stacking Energy Landscapes. *J. Chem. Inf. Model.* **2014**, *54* (5), 1371–1379. https://doi.org/10.1021/ci500183u.

(51)   David, J. G.; Hallam, H. E. Hydrogen-Bonding Studies of Thiophenols. *Spectrochim. Acta* **1965**, *21* (4), 841–850. https://doi.org/10.1016/0371-1951(65)80041-8.

**Figure 1**. The parallel displaced isomers of the thiophenol dimer compared with the dimers of phenol and aniline. Relative complexation energies (kJ mol$^{-1}$) and S-H$\cdots$S hydrogen bond distances (B2PLYP-D3(BJ)/def2-TZVP, Table 1) are given for the thiophenol dimer.
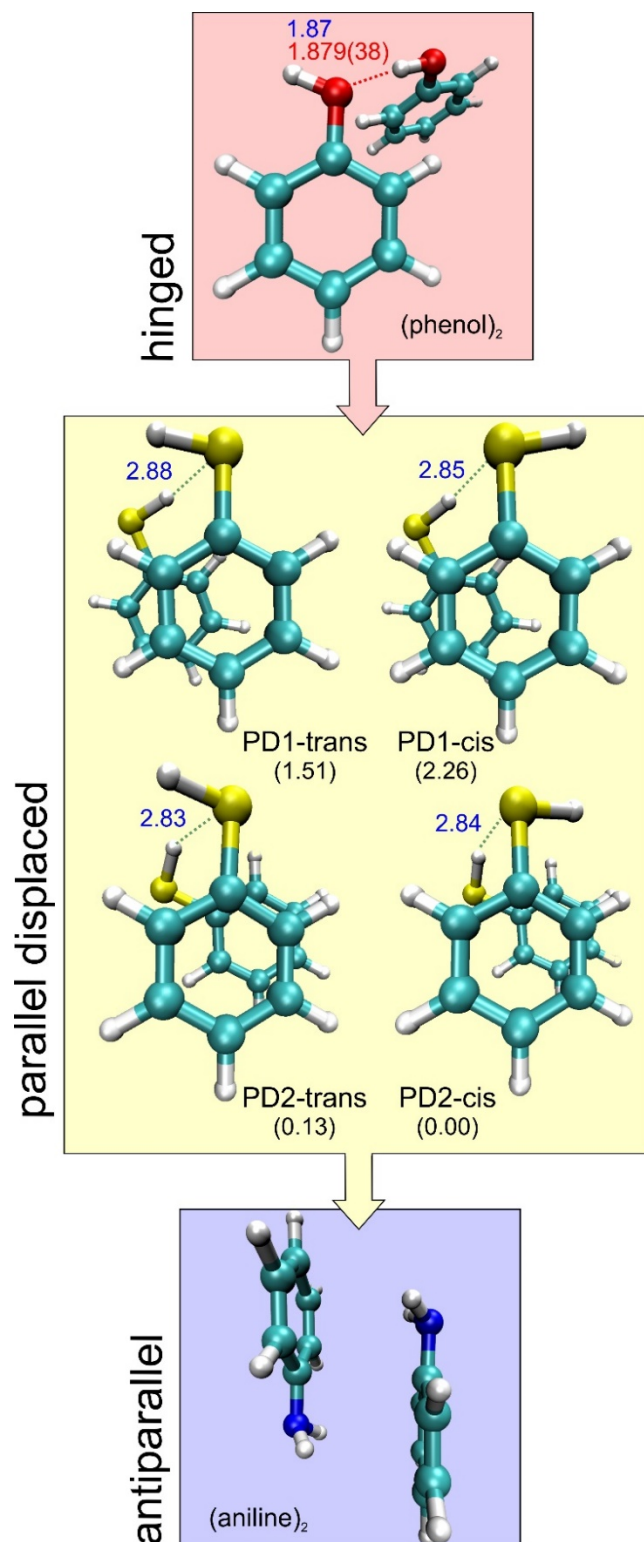
**Figure 2**. The microwave spectrum of thiophenol and its aggregates, illustrating typical rotational transitions of the dimer (see also Fig. S1).
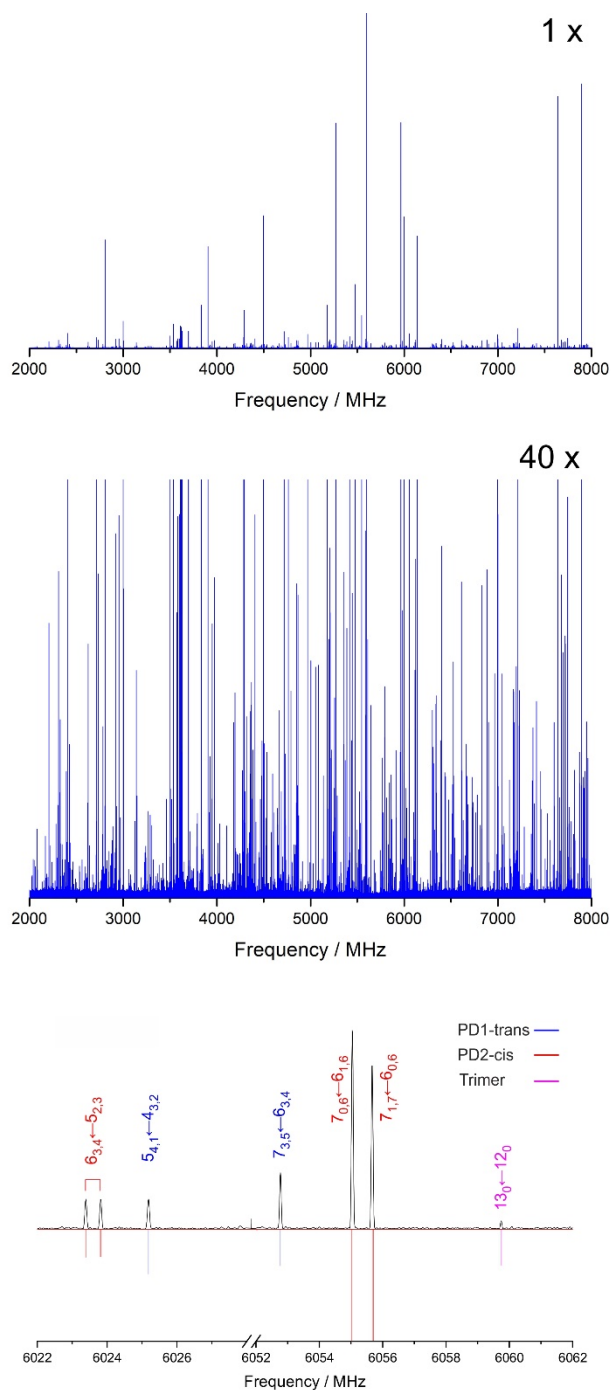
**Figure 3**. A 30 MHz section of the rotational spectrum of the thiophenol dimer, showing the disappearance of isomer I (PD1) when the neon carrier gas is replaced by argon, enforcing conformational relaxation to the global minimum PD2.
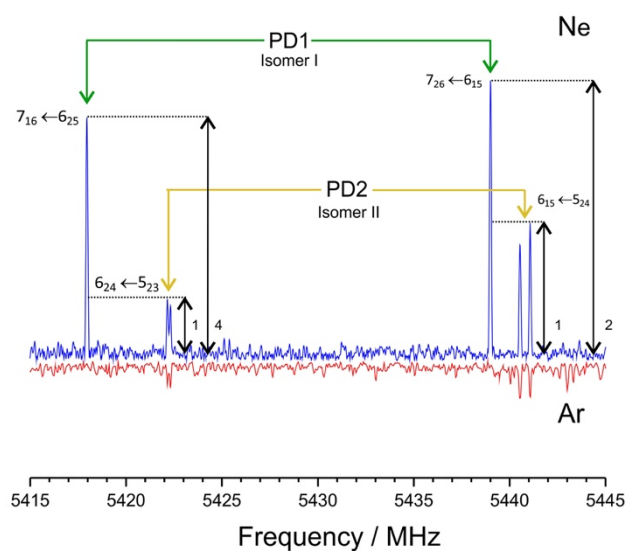
**Figure 4**. Mapping of non-covalent interactions in the most stable (PD2-*cis*) dimer structure of the thiophenol dimer and comparison of the reduced gradient with the phenol dimer.
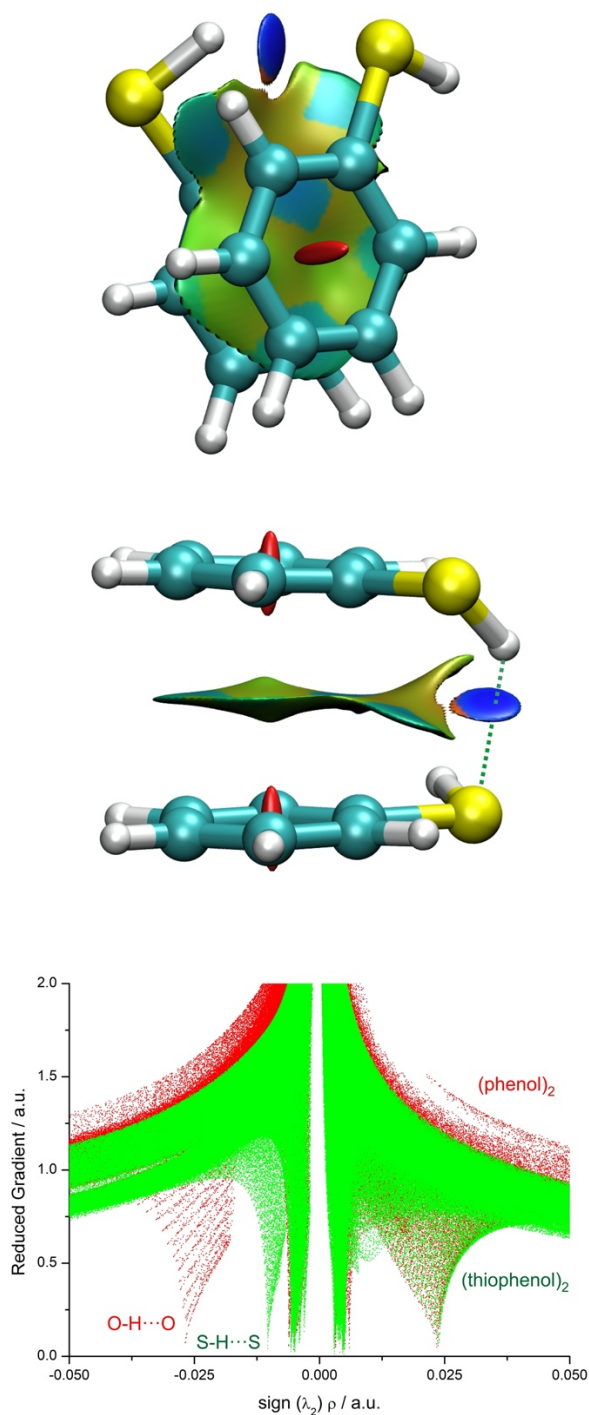
**Figure 5**. NCI plots for the $C_3$-symmetric structures of the trimers of aniline (left), phenol (center) and thiophenol (right, hydrogen bond distances according to B2PLYP-D3(BJ)).
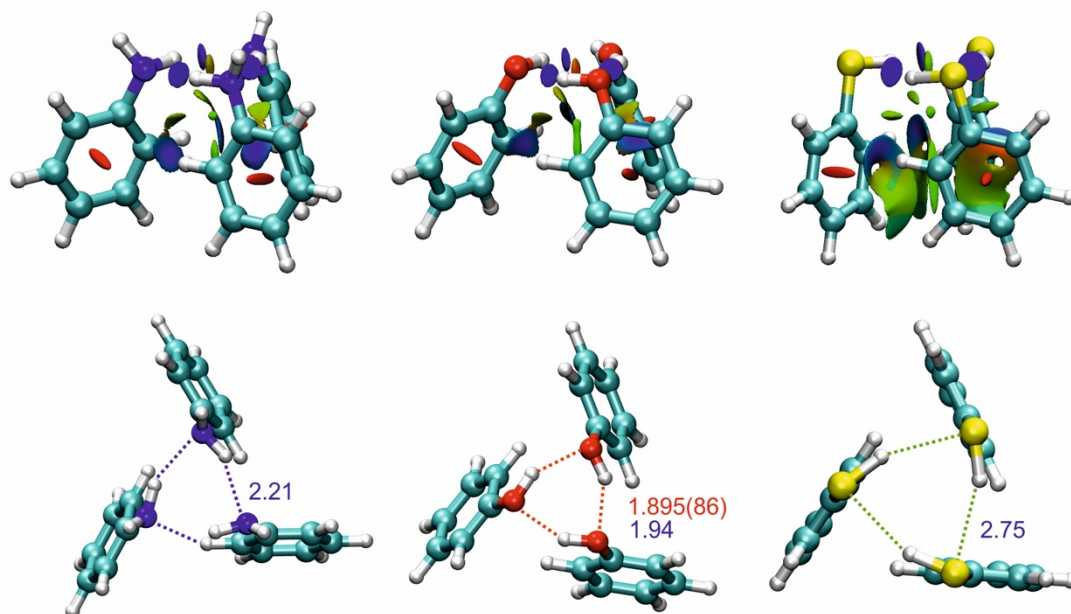
**Figure 6**. A radar chart showing the SAPT2+(3) binding energy decomposition for the thiophenol dimers (PD1-*trans* and PD2-*cis*) and comparison with the dimers of phenol, aniline, water, hydrogen sulfide, and pyridine-methane reported in Table S16 (SI).
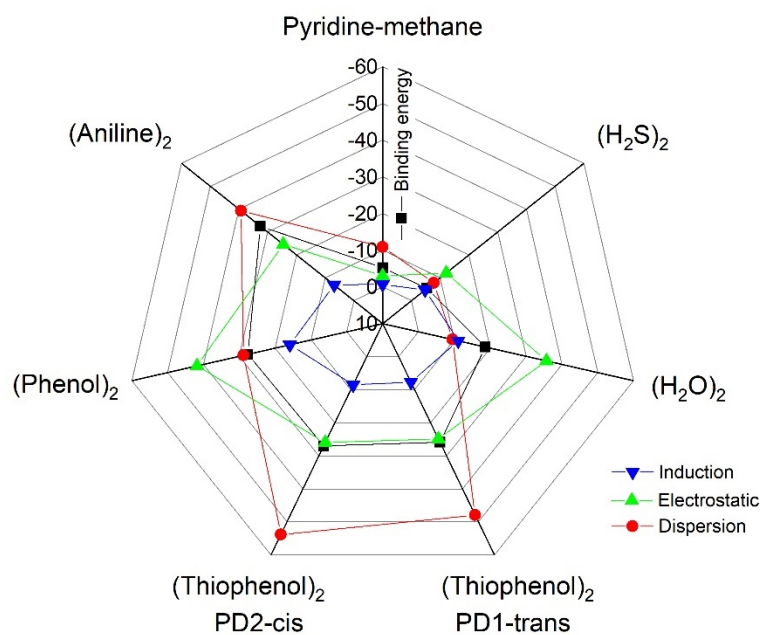
**Table 1**. Rotational parameters for the two isomers of the thiophenol dimer.

| | Experiment | | | Theory[g] | | | |
|---|---|---|---|---|---|---|---|
| | Isomer I | Isomer II[a] | | PD1-*trans* | PD1-*cis* | PD2-*cis* | PD2-*trans* |
| | | v=0 | v=1 | | | | |
| $A$ / MHz[b] | 662.74850(27)[f] | 626.72005(70) | 626.71915(70) | 693.6 | 690.4 | 628.4 | 629.7 |
| $B$ / MHz | 499.49241(20) | 511.48422(83) | 511.48295(83) | 496.3 | 496.9 | 527.6 | 530.3 |
| $C$ / MHz | 338.59668(19) | 422.94594(94) | 422.90305(91) | 347.3 | 348.9 | 435.8 | 435.6 |
| $\kappa$ | -0.01 | -0.13 | | -0.14 | -0.13 | -0.05 | -0.02 |
| $\Delta_J$ / kHz | 0.1611(13) | 0.1884(99) | | 0.355 | 0.329 | 0.077 | 0.094 |
| $\Delta_{JK}$ / kHz | 28.7175(37) | 0.090(41) | | -0.527 | -0.402 | 0.297 | 0.225 |
| $\Delta_K$ / kHz | -28.7008(36) | -0.199(38) | | 0.217 | 0.121 | -0.312 | -0.253 |
| $\delta_J$ / kHz | 0.05185(50) | -0.0276(47) | | 0.041 | 0.030 | -0.024 | -0.022 |
| $\delta_K$ / kHz | 14.1665(20) | 0.330(28) | | 0.054 | 0.150 | 0.495 | 0.446 |
| $\Delta E_{10}$ / MHz | | 8.8698(51) | | | | | |
| $N$[c] | 145 | 139 | | | | | |
| $\sigma$ / kHz | 7.6 | 19.8 | | | | | |
| $\|\mu_a\|$ / D[d] | Not detected | Not detected | | 0.1 | 0.5 | 0.0 | 0.8 |
| $\|\mu_b\|$ / D | Detected | Detected | | 1.5 | 2.1 | 1.6 | 1.1 |
| $\|\mu_c\|$ / D | Not detected | Detected | | 0.4 | 0.9 | 1.1 | 0.2 |
| $\Delta E$ / kJ mol$^{-1}$ [e] | | | | 0.85 | 1.56 | 0.00 | 0.42 |
| $\Delta G_{100 K}$ / kJ mol$^{-1}$ | | | | 0.03 | 0.73 | 0.00 | 0.42 |
| $\Delta G_{298 K}$ / kJ mol$^{-1}$ | | | | 0.00 | 0.54 | 1.87 | 2.42 |
| $\Delta E_c$ / kJ mol$^{-1}$ | | | | -25.77 | -25.02 | -27.15 | -27.28 |
| $r$(S-H $\cdots$ S) / Å | | | | 2.879 | 2.846 | 2.843 | 2.830 |
| $\angle$ (S-H$\cdots$S) / deg | | | | 138.9 | 140.8 | 134.5 | 134.0 |

[a]Torsional substates denoted v=0 and 1. [b]Rotational constants ($A$, $B$, $C$), Ray's asymmetry parameter ($\kappa=(2B-A-C)/(A-C)$), Watson's A-reduction centrifugal distortion constants ($\Delta_J$, $\Delta_{JK}$, $\Delta_K$, $\delta_J$, $\delta_K$) and torsional energy diference ($\Delta E_{10}$). [c]Number of transitions ($N$) and rms deviation ($\sigma$) of the fit. [d]Electric dipole moments ($\mu_a$, $\alpha = a$, $b$, $c$). [e]Relative energies corrected with the zero-point energy (ZPE), Gibbs energy ($\Delta G$) at 100 K and 298 K (1 atm) and complexation energy ($\Delta E_c$). [f]Standard errors in units of the last digit. [g]B2PLYP-D3(BJ)/def2-TVZP predictions, see SI for B3LYP-D3(BJ) and ωB97XD/cc-PVTZ values.

**Table 2**. Rotational parameters for the thiophenol trimer.

| | Experiment | Theory[b] | |
|---|---|---|---|
| | Isomer 1 | UUU | UUD |
| $A$ / MHz[a] | | 236.3 | 243.2 |
| $B$ / MHz | 233.07124(18) | 236.1 | 231.8 |
| $C$ / MHz | | 201.1 | 193.2 |
| $\kappa$ | | 0.99 | 0.54 |
| $\Delta_J$ / kHz | 0.0123(45) | 0.011 | 0.011 |
| $\Delta_{JK}$ / kHz | | 0.049 | 0.017 |
| $\Delta_K$ / kHz | | -0.055 | -0.021 |
| $\delta_J$ / kHz | | 0.000 | 0.002 |
| $\delta_K$ / kHz | | -0.072 | 0.038 |
| $|\mu_a|$ / D | | 0.0 | 0.5 |
| $|\mu_b|$ / D | | 0.0 | 0.3 |
| $|\mu_c|$ / D | | 3.1 | 0.8 |
| $N$ | 13 | | |
| $\sigma$ / kHz | 5.8 | | |
| $\Delta E$/kJ mol$^{-1}$ | | 0 | -0.71 |
| $\Delta G_{100\,K}$ / kJ mol$^{-1}$ | | 0 | -0.06 |
| $\Delta G_{298\,K}$ / kJ mol$^{-1}$ | | 0 | -0.06 |
| $\Delta E_c$ / kJ mol$^{-1}$ | | -68.07 | -67.82 |
| $r$(S-H $\cdots$ S) / Å | | 2.746-2.760 | 2.758 |
| $\angle$(S-H$\cdots$S) / $deg$ | | 154.3-155.6 | 157.8 |

[a]Parameter definition as in Table 1. [b]See Table S3 (SI) for notation.